Eur. Phys. J. B (2023)96:155
https://doi.org/10.1140/epjb/s10051-023-00625-9

THE EUROPEAN PHYSICAL JOURNAL B

Regular Article - Solid State and Materials

Monte Carlo simulation of hard-, square-well, and square-shoulder disks in narrow channels

Riccardo Fantoni[a]

Dipartimento di Fisica, Università di Trieste, strada, Costiera 11, Grignano, 34151 Trieste, Italy

Received 5 October 2023 / Accepted 17 November 2023

Abstract. We perform Monte Carlo simulation of the thermodynamic and structural properties of hard-, square-well, and square-shoulder disks in narrow channels. For the thermodynamics, we study the internal energy per particle and the longitudinal and transverse compressibility factor. For the structure, we study the transverse density and density of pairs profiles, the radial distribution function and longitudinal distribution function, and the (static) longitudinal structure factor. We compare our results with a recent exact semi-analytic solution found by Montero and Santos for the single file formation and first nearest neighbor fluid, and explore how their solution performs when these conditions are not fulfilled making it just an approximation.

1 Introduction

Confined fluids are an important field of study due to the wide range of applications and situations where they can be found [1]. Interesting systems in physics, chemistry, or biology involve dealing with confined particles. Examples are carbon nanotubes [2,3] or biological ion channels [4]. In many of these systems, the geometry is so restrictive that one or more spatial dimensions become negligible. One can, therefore, often describe these systems as living in a one (1D) or two (2D) dimensional space to simplify the mathematical model and its subsequent study. Yet, in some cases, it is necessary a more realistic description which can be obtained by modeling the geometrical restriction without recurring to a dimensionality reduction. So, for particles living in three dimensions, we will talk about *quasi* two-dimensional (quasi 2D) or *quasi* one-dimensional (quasi 1D) fluids. In this work, we will study particles living in 2D which are quasi 1D.

Despite its clear importance, systems whose structural properties are amenable to exact analytic solutions are very scarce, and usually limited to 1D fluids [5–14] with only nearest neighbor interactions [15–17]. Even if for restricted values of the thermodynamic parameters, even 2D fluids may offer an exact analytic classical equilibrium statistical mechanics solution [18–21]. Otherwise, one must resort to approximations, numerical methods, or simulations.

Recently, Montero and Santos [22,23] developed an exact semi-analytic formalism able to solve the *longitudinal* structure and thermodynamics of a quasi 1D problem of *single file* formation and *first nearest neighbor* fluids of *hard-core* particles in *narrow channels*.

In particular, the single file confinement constraint [24,25] implies that particles are inside a *pore* that is not wide enough to allow particles to bypass each other, therefore confining them into a single file formation.

Whereas, the first nearest neighbor constraint implies that the particles are not allowed to interact with their second (or beyond) nearest neighbors [14].

The pore is a 2D narrow channel or band with *periodic boundary conditions* along the longitudinal direction and *open boundary conditions* along the transverse direction where the particles are assumed to be confined by *hard walls*.

The nearest neighbor constraint allows the use of the exact solution that is available for 1D fluids subject to such constraint [15–17]. In fact, Montero and Santos study their quasi 1D fluids of particles interacting through a *pairwise* potential $\varphi_{2D}(r)$ with a mapping to a 1D *non-additive* mixture [26] of equal chemical potentials species, where the species index i denotes those particles with the ordinate equal to a fixed value within the channel and the interaction potential becomes $\varphi_{ij}(x) = \varphi_{2D}(\sqrt{x^2+(y_i-y_j)^2})$. They further assume the mixture to be *polydisperse* [27–29], so that the molar fraction x_i of the ith species can be rewritten as $F(y)\mathrm{d}y$ which represents the fraction of particles with the ordinate lying in the interval $[y, y+\mathrm{d}y]$. What they find [30] is that working in the isothermal isobaric ensemble, the average of a function of y can be expressed as $\langle f(y)\rangle = \int \mathrm{d}y\, F(y) f(y)$, where $F(y) = \phi^2(y)$. Here $\phi(y)$ is the eigenfunction of the

[a] e-mail: riccardo.fantoni@posta.istruzione.it (corresponding author)

Published online: 28 November 2023

maximum eigenvalue of a certain operator $K(y_1, y_2) = \exp\{-\beta P_{\rm L}\sigma(y_1, y_2) - \frac{1}{2}\beta[\Phi_{\rm ext}(y_1) + \Phi_{\rm ext}(y_2)]\}$, where $\beta = 1/k_{\rm B}T$ with $k_{\rm B}$ Boltzmann constant and T the absolute temperature, $P_{\rm L}$ is the longitudinal pressure, $\sigma(y_1, y_2)$ is the distance of closest approach of particles 1 and 2, which are nearest neighbors, and $\Phi_{\rm ext}(y)$ is the external potential which acts only in the dimension of the y coordinates and confines the particles within the channel.

In this work, we will perform Monte Carlo (MC) simulations [31,32], in the *canonical ensemble* (for results using molecular dynamics see Ref. [33]), to study the thermodynamic and structural properties of Hard (HD), Square-Well (SW), and Square-Shoulder (SS) disks in narrow channels. For the thermodynamics, we will study the internal energy and the compressibility factor. For the structure, we will study the Transverse Density Profile (TDP), the Transverse Density of Pairs Profile (TDPP), the Radial Distribution Function (RDF) and Longitudinal Distribution Function (LDF), and the (static) Longitudinal Structure Factor (LSF).

Of course with our MC simulations, we are not bound to fulfill the single file and nearest neighbor constraints. We will, therefore, also study the performance of the solution of Montero and Santos outside the nearest neighbor regime where it is expected to be just an approximation.

The work is organized as follows: In Sect. 2, we will describe the mathematical model of the physical fluid of interest, the MC estimators for the quantities we want to measure in our computer experiments, and some MC results for the thermodynamics. In Sect. 3, we present our MC results for the structure. Section 4 is for concluding remarks.

2 Model and simulation details

Consider a 2D system of N particles interacting via a *pairwise potential* $\varphi_{\rm 2D}(r)$. The particles are confined in a very long channel of width $w = 1 + \epsilon$ and length $L \gg w$, in such a way that they are in *single file* formation and only *first nearest neighbor* interactions take place. The *channel surface density* of the fluid will be $\sigma = N/Lw = \lambda/w$ with λ the *longitudinal density*. The total potential energy of the fluid will be

$$\Phi(\mathbf{Q}) = \frac{1}{2}\sum_{i,i\neq j}\varphi_{\rm 2D}(q_{ij}) + \Phi_{ext}, \tag{2.1}$$

where $\mathbf{Q} = (\mathbf{q}_1, \mathbf{q}_2, \ldots, \mathbf{q}_N)$ are the positions of the particles in the channel and $\mathbf{q} = (x, y)$ with $x \in [-L/2, L/2]$ and $y \in [-\epsilon/2, \epsilon/2]$. We have *periodic boundary conditions* (PBC) along x so that $x_i \to x_i - {\rm nint}(x_i/L)L$ where 'nint' is the nearest integer and enforce the usual minimum image convention so that $x_i - x_j \to x_i - x_j - {\rm nint}[(x_i - x_j)/L]L$. Along y, instead, we have *open boundary conditions* (OPC) where in particular we assume to have an infinitely repulsive *external potential* Φ_{ext} for $y > \epsilon/2$ and $y < -\epsilon/2$ and we do not employ the minimum image convention. We will denote with $q_{ij} = \sqrt{(x_i - x_j)^2 + (y_i - y_j)^2}$ the distance between particles at $\mathbf{q}_i$ and at $\mathbf{q}_j$.

For Hard Disks (HD), we have

$$\varphi_{\rm 2D}(r) = \begin{cases} \infty & \text{if } r < 1 \\ 0 & \text{else} \end{cases}. \tag{2.2}$$

If the transverse separation between two disks at contact is s, their longitudinal separation is

$$a(s) = \sqrt{1 - s^2}. \tag{2.3}$$

The single file constraint in this case requires clearly $\epsilon < \epsilon_{\rm sf} = 1$. In this case, we have a close packing limit longitudinal density given by $\lambda_{\rm cp} = 1/a(\epsilon)$. To enforce also the first nearest neighbor constraint we require $\epsilon < \epsilon_{\rm nn-HD} = \sqrt{3}/2$. For $\epsilon = \sqrt{3}/2$, the close packing longitudinal density is $\lambda_{\rm cp} = 2$ and the surface density is $\sigma_{\rm cp} = 2/(1 + \sqrt{3}/2) = 1.071\ldots$.

For Square-Wells (SW) or Square-Shoulders (SS), we have

$$\varphi_{\rm 2D}(r) = \begin{cases} \infty & \text{if } r < 1 \\ -\varphi_0 & \text{if } 1 < r < r_0 \\ 0 & \text{else} \end{cases}, \tag{2.4}$$

with $\varphi_0 > 0$ for SW and $\varphi_0 < 0$ for SS.

In this case, to enforce the first nearest neighbor constraint, we require $\epsilon < \epsilon_{\rm nn} = \sqrt{1 - (r_0/2)^2}$. Since $r_0 > 1$, we will have $\epsilon_{\rm nn} < \epsilon_{\rm nn-HD}$.

In our computer experiment, we measured various thermodynamic and structural properties of these fluids. We could than compare our numerical *meta data* with analytic or semi-analytic theoretical data available in the literature. To *measure* an observable $\mathcal{O}$, we need to calculate [34] the following quantity

$$\langle\mathcal{O}\rangle = \frac{\int O(\mathbf{Q})\exp[-\beta\Phi(\mathbf{Q})]\,{\rm d}\mathbf{Q}}{\int \exp[-\beta\Phi(\mathbf{Q})]\,{\rm d}\mathbf{Q}}, \tag{2.5}$$

where $\beta = 1/k_{\rm B}T$ with $k_{\rm B}$ Boltzmann constant and T absolute temperature. In our canonical (at fixed number of particles, surface area, and temperature) Monte Carlo (MC) simulation, we employed the usual M(RT)^2 algorithm [34] to sample the probability distribution $\propto \exp[-\beta\Phi(\mathbf{Q})]$.

We generally found it sufficient to use $N = 100$ with runs up to 10^9 MC single particle moves long. The spatial extent of the uniform particle displacement move was tuned so to have acceptance ratios around 1/2 and kept constant during the run, even if this was not always possible at high densities.

2.1 Structure

For the *Radial Distribution Function* (RDF) [35,36], $g(r) = \langle \mathcal{O} \rangle$, we have the following *histogram estimator*

$$O(\mathbf{Q}; r) = \sum_{i, i \neq j} \frac{1_{[r-\Delta/2, r+\Delta/2[}(q_{ij})}{N n_{\mathrm{id}}(r)}, \tag{2.6}$$

where Δ is the histogram bin, $1_{[a,b[}(t) = 1$ if $t \in [a, b[$ and 0 otherwise, and $n_{\mathrm{id}}(r)$ is the average number of particles on the interception of the circular crown $[r - \Delta/2, r + \Delta/2[$ with the part of the channel accessible to the particles centers, for the uniform gas at the same longitudinal density λ, which for a narrow channel can be approximated to

$$n_{\mathrm{id}} = 2\lambda\Delta \ , \tag{2.7}$$

independent of r. We have that $g(r)$ gives the probability density that sitting on a particle at $\mathbf{q}$ one has to find another particle at $\mathbf{q}'$, where $r = \sqrt{(x - x')^2 + (y - y')^2}$.

Instead of counting how many disks are separated a 2D distance r we can count how many are separated a 1D longitudinal distance $|x|$. So, doing the same calculation described above, but, in the end, keeping track only of the relative abscissas, $r = \sqrt{(x - x')^2} = |x - x'|$, of the particles, we find the quasi 1D or *Longitudinal Distribution Function* (LDF) $g(|x|)$.

The Fourier transform of the radial distribution function is the (static) structure factor $S(k)$ which for an isotropic system is given by

$$S(k) = 1 + \frac{\lambda}{\epsilon} \int [g(r) - 1] \exp(-i\mathbf{k} \cdot \mathbf{r}) \, \mathrm{d}\mathbf{r} + \frac{\lambda}{\epsilon} (2\pi)^2 \delta(\mathbf{k}), \tag{2.8}$$

where usually the Dirac delta function is neglected. Note also that from the definition (2.6) we find the following sum rule

$$\frac{\lambda}{\epsilon} \int [g(r) - 1] \, \mathrm{d}\mathbf{r} = -1, \tag{2.9}$$

and from the definition (2.8) follows $\lim_{k \to 0} S(k) = 0$. Moreover if $\lim_{r \to 0} g(r) = 0$ then $\lim_{k \to \infty} S(k) = 1$. Now for our quasi 1D geometry of the narrow channel, the isotropy is clearly lost and when we count just the longitudinal distances between the particles, for the LDF $g(|x|)$, we may still find $\lim_{k_x \to 0} S(k_x) \neq 0$ since the sum rule becomes $\frac{\lambda}{\epsilon} \int [g(|x|) - 1] \, \mathrm{d}x = -\frac{1}{\epsilon} < -1$. In the following, we will always refer to this *Longitudinal Structure Factor* (LSF) $S(k_x)$ and for brevity, we will simply rewrite $k_x \to k$.

Another structural property to study is the *Transverse Density Profile* (TDP) $F(y)$ such that $F(y)\mathrm{d}y$ gives the fraction of particles with the ordinate in the interval $[y, y + \mathrm{d}y]$. By symmetry, we clearly must have for F an even function. A related function is $F_2(y)$, the fraction of pairs of different particles 1 and 2 such that their transverse distance $|y_2 - y_1| \in [y, y + \mathrm{d}y]$. We will call this the *Transverse Density of Pairs Profile* (TDPP).

2.2 Internal energy

For the *internal energy per particle* of the fluid [35,36], we have $u = \langle \mathcal{O} \rangle$ with the following internal energy per particle *estimator*

$$O(\mathbf{Q}) = \Phi(\mathbf{Q})/N. \tag{2.10}$$

For SW/SS with $|\beta\varphi_0| = 1$, we found the results of Table 1.

2.3 Compressibility factor

For the compressibility factor $Z = \beta P/(\lambda/\epsilon)$ of the confined 2D fluid, we have, from the virial theorem [37]

$$\begin{aligned} Z &= 1 - \beta \frac{\lambda}{\epsilon} \frac{1}{4} \iint_{\substack{x_1, x_2 \in [-L/2, L/2] \\ y_1, y_2 \in [-\epsilon/2, \epsilon/2]}} r\varphi'_{2\mathrm{D}}(r) g(\mathbf{r}) \, \mathrm{d}\mathbf{r} \\ &\approx 1 + \frac{\lambda}{2} \int_0^\infty \frac{\mathrm{d} \exp[-\beta\varphi_{2\mathrm{D}}(r)]}{\mathrm{d}r} r y(r) \, \mathrm{d}r \\ &= 1 + \frac{\lambda}{2} [g(1^+) + (1 - e^{\beta\varphi_0}) r_0 g(r_0^+)], \end{aligned} \tag{2.11}$$

where in the first line $\mathrm{d}\mathbf{r} = \mathrm{d}(x_1 - x_2)\mathrm{d}(y_1 - y_2)$, $g(\mathbf{r}) = g(|x_1 - x_2|; y_1, y_2)$, and we used polar coordinates so that $\mathrm{d}\mathbf{r} = r\mathrm{d}\theta\mathrm{d}r$. In the second line, we approximated $\int_{\mathrm{channel}} r\mathrm{d}\theta \approx 2\epsilon$ for the narrow channel, we then introduced the continuous indirect correlation function $y(r) = g(r) \exp[-\beta\varphi_{2\mathrm{D}}(r)]$, where $g(r)$ is the 2D RDF of Eq. (2.6), and used the fact that for the SW/SS pair potential of Eq. (2.4), we have

$$\frac{\mathrm{d} \exp[-\beta\varphi_{2\mathrm{D}}(r)]}{\mathrm{d}r} = e^{\beta\varphi_0} \delta(r - 1) + (1 - e^{\beta\varphi_0}) \delta(r - r_0). \tag{2.12}$$

The total thermodynamic pressure $P = (P_{\mathrm{L}} + P_{\mathrm{T}})/2$, where P_{L} and P_{T} are the *longitudinal and transverse 2D pressures*, respectively. In Table 1, we present some results for SW/SS.

Let us now specialize to the HD case so that $\varphi_0 = 0$. We will also introduce $p = P_{\mathrm{L}}\epsilon$. From the Table I of Ref. [22], we find that $Z_{\mathrm{L}}^{\mathrm{exact}} = \beta p/\lambda = 12.774$ when $\epsilon = 0.4$ and $\beta p = 12$. From these data, we extract $\lambda = \beta p / Z_{\mathrm{L}}^{\mathrm{exact}} = 0.671w$ and, at this longitudinal density, our canonical simulation gives $\beta P = 15.85(2)$ for $\Delta = 10^{-2}$ and $\beta P = 16.53(1)$ for $\Delta = 10^{-3}$. Since the exact longitudinal pressure is $\beta P_{\mathrm{L}}^{\mathrm{exact}} = \beta p/\epsilon = 30$, we estimate a transverse pressure of $\beta P_{\mathrm{T}} \approx 2(16.53) - 30 = 3.06$. For the case when $\epsilon = 0.8$ and $\beta p = 12$, we find $\beta P = 14.46(1)$ (these measures tend to slightly increase even further at lower Δ). See Table 2 for these Z measurement. Exact results from the Montero and Santos

Table 1 Internal energy per particle (2.10) and total pressure (2.11) for $N = 100$ SW/SS with $|\beta\varphi_0| = 1$. The results were determined from runs made of 5×10^7 single particle moves

ϵ	r_0	$\lambda_{\rm cp}$	λ	σ	u		βP	
					SW	SS	SW	SS
4/5	6/5	1.66667	1.080	0.6	−0.9303(4)	+0.7673(7)	7.351(1)	9.965(3)
4/5	6/5	1.66667	1.260	0.7	−0.9797(4)	+0.9176(8)	14.653(4)	16.45(1)
$\sqrt{7}/4$	3/2	1.33333	0.997	0.6	−0.99837(2)	+0.9895(2)	9.865(2)	10.160(2)
$\sqrt{7}/4$	3/2	1.33333	1.163	0.7	−0.9999989(6)	+0.99998(1)	23.856(7)	23.12(2)

Table 2 Results for $N = 100$ HD from Eqs. (2.11) and (2.13a) and comparison with the exact values of Table I of Ref. [22]. $Z_{\rm L}^{\rm Mon}$ are the MC values of Ref. [31]. The two low-density cases were determined from runs made of 5×10^7 single particle moves, $\Delta = 10^{-5}$ for $Z_{\rm L}$, and $\Delta = 10^{-3}$ for Z

ϵ	p	$Z_{\rm L}^{\rm exact}$	$Z_{\rm L}^{\rm Mon}$	λ	λ/ϵ	$\lambda_{\rm cp}$	$2 + a(\epsilon)p$	Z	$Z_{\rm L}$	$Z_{\rm L}^{\rm exact}/Z_{\rm L}$	$\lambda(I_0 - I_0^{\rm asy})$	$\lambda^2(I_1 - I_1^{\rm asy})$
0.4	12	12.774	12.774	0.939408	2.34852	1.09109	12.998	7.04(1)	12.8094(3)	0.997	2.1	2.3
0.4	120	112.04	112.03	1.07105	2.67762	1.09109	111.98	–	?	?	$+3.6 \times 10^{-4}$	$+3.5 \times 10^{-4}$
0.8	12	9.6547	9.6548	1.24292	1.55365	1.66667	9.2000	9.31(1)	9.780(4)	0.987	-2.4×10^{-2}	-2.5×10^{-2}
0.8	120	74.017	74.016	1.62125	2.02656	1.66667	74.000	–	?	?	$< 10^{-15}$	-4.9×10^{-6}

analysis [38] give $\beta P = 16.722$ for $\epsilon = 0.4, \beta p = 12$ and $\beta P = 14.8551$ for $\epsilon = 0.8, \beta p = 12$. Alternatively, one can use the canonical ensemble exact expression found by Pergamenshchik [39].

Alternatively, one can use the quasi 1D scenario and the LDF $g(|x|)$ to find the longitudinal compressibility factor $Z_{\rm L} = \beta P_{\rm L}/(\lambda/\epsilon)$. To do this, we need to calculate (see Appendix A [40])

$$Z_{\rm L} = \frac{1 - \lambda I_0}{1 - \lambda + \lambda^2 (I_0 - I_1)}, \tag{2.13a}$$

$$I_n = \int_{a(\epsilon)}^{1} x^n g(x)\, {\rm d}x. \tag{2.13b}$$

We computed the integrals I_n for $n = 0, 1$ numerically with a discretization Δ on the abscissa $x^i = \Delta i$ with $i = 0, 1, 2, 3, \ldots$. In Table 2, we show our results compared with the ones of Ref. [22]. Note that for the two high-density cases, this way of estimating numerically $Z_{\rm L}$ is not useful since for $\lambda \to \lambda_{\rm cp}$ we find

$$\lambda I_0 \to 1 - 8 \exp\{-\beta p[1 - a(\epsilon)]\} = \lambda I_0^{\rm asy},$$

$$\lambda^2 I_1 \to 1 - \frac{1}{2}\{1 + [2 - a(\epsilon)]\lambda\}(1 - \lambda I_0^{\rm asy}) \tag{2.14a}$$

$$= \lambda^2 I_1^{\rm asy}, \tag{2.14b}$$

and both numerator and denominator in Eq. (2.13a) vanish. In this case, one can use the analytic expression (see Appendix C of Ref. [22])

$$Z_{\rm L} \to 2 + a(\epsilon)p = \frac{2}{1 - \lambda/\lambda_{\rm cp}}, \tag{2.15}$$

valid asymptotically for λ near to its close packing limit $\lambda_{\rm cp}$.

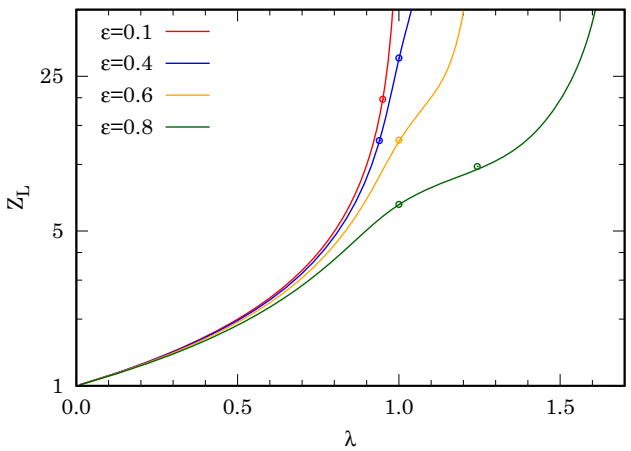

Fig. 1 Comparison between our MC (points) and the exact results (lines) of Ref. [22] for the longitudinal compressibility factor. The statistical error in the MC points is smaller than the point symbol. The MC simulations were up to 10^9 single particle moves long

Additional points are presented in Fig. 1, where we compare with the exact results of Ref. [22] (results shared privately and not all previously published). We found that at the same value of λ, it takes longer to equilibrate the large ϵ cases. For example, the MC points at $\epsilon = 0.1$ required just 10^7 single particle moves; whereas, the ones at $\epsilon = 0.8$ required up to 10^9 moves (Figs. 2, 3).

Note that a drawback of this way of estimating the longitudinal pressure is that it is hard to tell if the statistical error is more or less important than the systematic error due to the choice of the discretization Δ. In this respect, instead of working in the canonical $N\lambda T$ ensemble, it would be desirable to work in the isother-

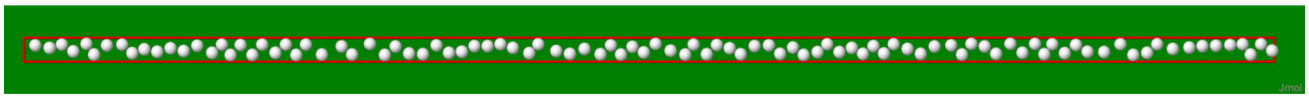

Fig. 2 Snapshot of the simulation box for $N = 100$ HD of radius $r_0 = 1$ with $\epsilon = \sqrt{3}/2$ and $\lambda = 1$

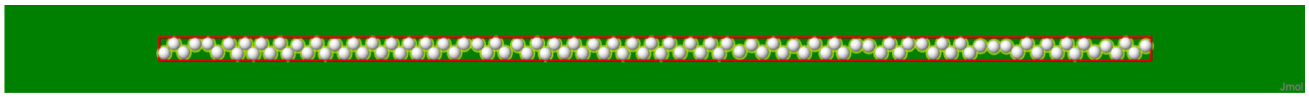

Fig. 3 Snapshot of the simulation box for $N = 100$ SW with $\beta\varphi_0 = 1$ and radius $r_0 = 6/5$ with $\epsilon = 4/5$ and $\sigma = 7/10$

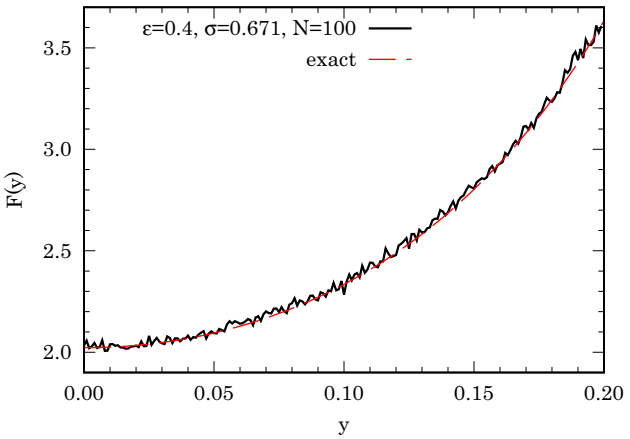

Fig. 4 TDP for $N = 100$ HD with $\epsilon = 0.4$ and $\lambda = 0.671w$. The exact result, shared privately by A. Montero and not published before, fits our MC results very well. In particular from Fig. 4 of Ref. [22], we see how the particles tend to escape from the center of the channel preferring to stay in contact with the walls as density approaches the packing density

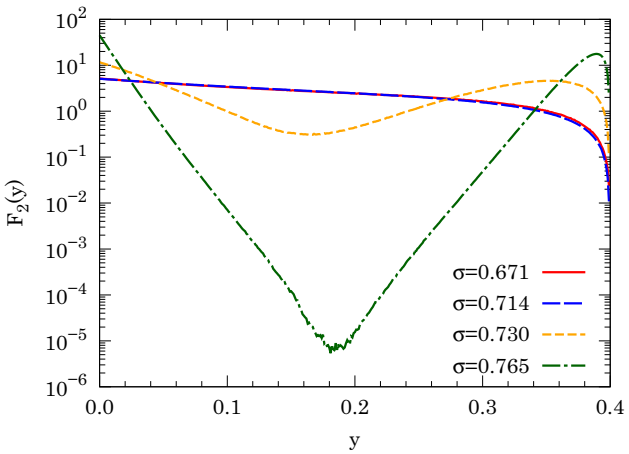

Fig. 5 TDPP for $N = 100$ HD with $\epsilon = 0.4$ and $\sigma = 0.671, 0.714, 0.730, 0.765$ corresponding to $\lambda = 0.939, 1.000, 1.022, 1.071$, respectively. We can see how this density function starts changing only really near to the close packing density $\lambda_{\rm cp} = 1.091$, when the TDP becomes very small at $y \approx 0$

mal isobaric NpT ensemble with a volume change move where one only varies the length of the channel L.

For the HD case, with $\epsilon = 0.4$ and $\lambda = 0.671w$, we find the TDP $F(y)$ shown in Fig. 4. As you can see the exact result of Ref. [22] fits our MC data very well. For the same case the TDPP, $F_2(y)$, is shown in Fig. 5. From this figure, we can see how the TDPP changes drastically only getting really near to the close packing density $\lambda_{\rm cp} = 1.091$.

3 Results for the structure

In this section, we present our MC results for the structural properties of the confined quasi 1D fluids of our interest.

3.1 Ideal gas (id)

We first tried to switch off the pair potential between the particles taking $\varphi_{2D}(r) = 0$ but keeping the confining infinitely repulsive external potential $\Phi_{\rm ext}$ switched on. For the case $\lambda = \sigma w = 1$ and $\epsilon = \sqrt{3}/2$ we found the results for the LDF and RDF shown in Figs. 6 and 7, respectively. As you can clearly see from the MC results, the LDF, and as a consequence the LSF, is uniform but the RDF is not.

Note that this is just an effect of the geometry of the confinement in fact using periodic boundary conditions also along the transverse, y, direction one gets both a uniform LDF and RDF as expected. Moreover, the TDP turns out to be uniform $F(y) = 1/\epsilon$ irrespective of using open or periodic boundary conditions along the transverse direction.

For the case of our interest, with periodic boundary conditions along x and open boundary conditions along y, the RDF can be calculated exactly analytically as follows (see Appendix B [40])

$$g_{\rm id}(r) = \frac{2r}{\epsilon} \begin{cases} \pi/2 - r/\epsilon & r < \epsilon \\ \sqrt{(r/\epsilon)^2 - 1} - r/\epsilon + \arctan[1/\sqrt{(r/\epsilon)^2 - 1}] & \text{else} \end{cases} . \tag{3.1}$$

3.2 Hard disks (HD)

We tried to reproduce the case $\epsilon = \sqrt{3}/2, \lambda = \sigma w = 1$ of Fig. 5(a) of Ref. [23]. Our results for the LDF, LSF,

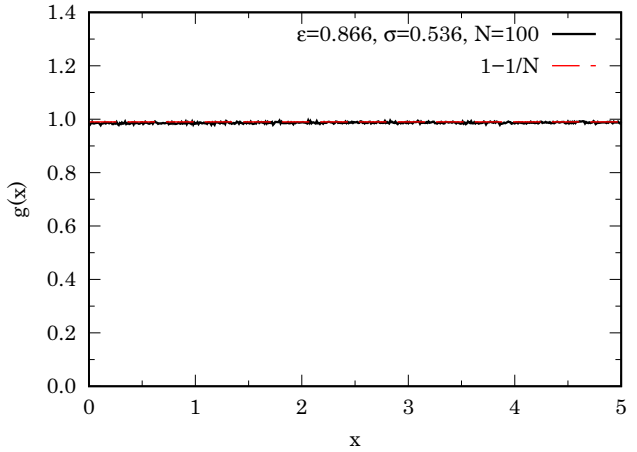

Fig. 6 LDF for the ideal gas with $\lambda = 1$ and $\epsilon = \sqrt{3}/2$. The MC data are fitted very well by the exact result of $g_{\rm id}(x) = 1 - 1/N$

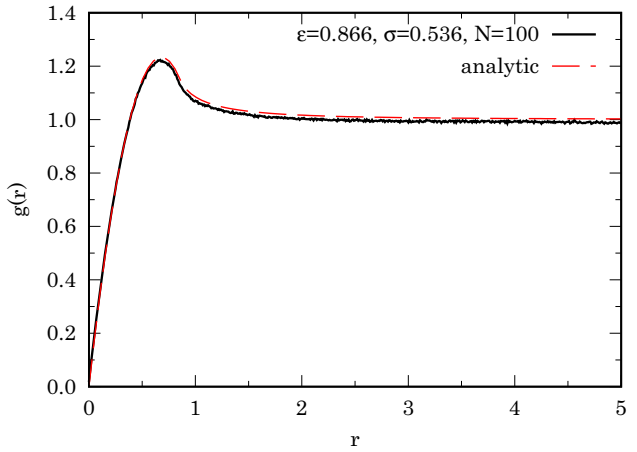

Fig. 7 RDF for the ideal gas with $\lambda = 1$ and $\epsilon = \sqrt{3}/2$. Here, the $g(r)$ is calculated from Eq. (2.6) using for $n_{\rm id}(r)$ its asymptotic value $2\lambda\Delta$ everywhere. The analytic result is the one in the thermodynamic limit of Eq. (3.1). The slight discrepancy is the expected finite size effect. Remember that $\lim_{r\to\infty} g_{\rm id}(r) = 1 - 1/N$

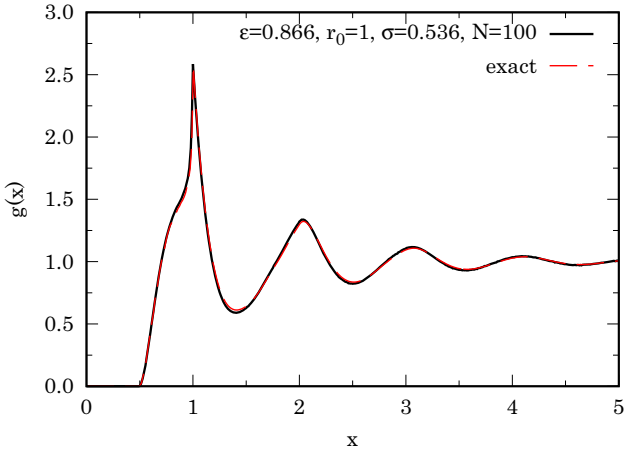

Fig. 8 LDF for $N = 100$ HD of radius $r_0 = 1$ with $\epsilon = \sqrt{3}/2$ and $\lambda = 1$. Our MC data are fitted very well by the exact result of Ref. [23] which is in the thermodynamic limit

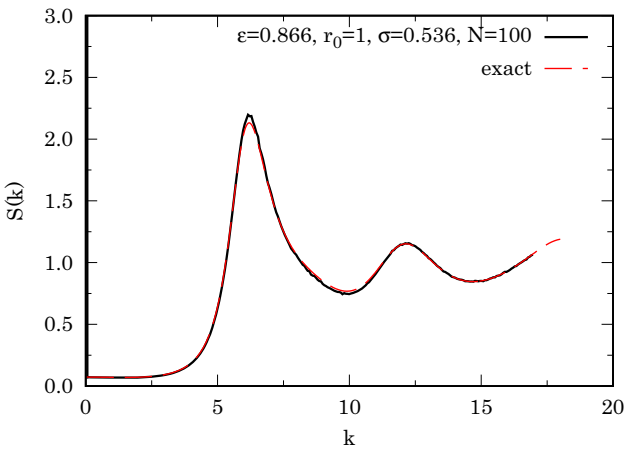

Fig. 9 LSF for $N = 100$ HD of radius $r_0 = 1$ with $\epsilon = \sqrt{3}/2$ and $\lambda = 1$. We used $2n_{\rm max} + 1$ wave numbers with $n_{\rm max} = 270$. The exact result in the thermodynamic limit, shared privately by A. Montero and not published before, fits our MC results very well

and RDF are shown in Figs. 8, 9, and 10, respectively. In Fig. 2, we show a snapshot of the simulation box.

We also run simulations for the cases considered in Fig. 10 of Ref. [23]. The results are shown in Fig. 10. Comparison with the work of Montero and Santos [23] shows that our RDF is different from what they define as g_{2D} [40].

It is interesting to study how the solution of Montero and Santos [23] performs outside of the nearest neighbor regime where it is expected to be not exact anymore. Such a study was carried out at the level of the compressibility factor in Fig. 7 of Ref. [22]. We want here to repeat it for the structure. In Fig. 11 we show the comparison for the LDF between our exact MC simulations and the approximate solution of Montero and Santos for HD at $\lambda = 1.2$ and $\epsilon = 0.9, 1.0, 1.118$. From the comparison, we see that the solution of Montero & Santos, which is exact for $\epsilon \le \epsilon_{\rm nn-HD}$, is a rather good approximation for $\epsilon_{\rm nn-HD} < \epsilon < \epsilon_{\rm sf}$, but it becomes a poor approximation for $\epsilon \ge \epsilon_{\rm sf}$. The breakdown of their solution at $\epsilon > 1$ manifests itself through an LDF that does not follow the exact result from the MC simulation. This confirms the findings of Kofke and Post [30].

It is interesting to note that Hu and Charbonneau [41] have shown how the envelope of the LDF $g(x) - 1$ has an exponential decay at large distances.

3.3 Square-wells (SW) and square-shoulders (SS)

For SW/SS, we explored the following two limiting nearest neighbor cases considered in Table 1, namely:

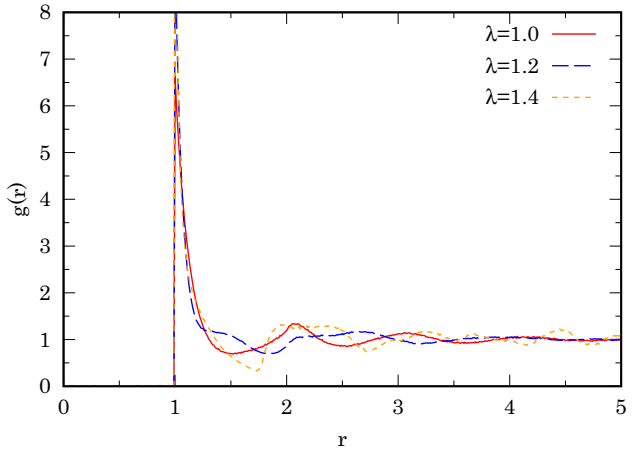

Fig. 10 RDF for $N = 100$ HD of radius $r_0 = 1$ with $\epsilon = \sqrt{3}/2$ and $\lambda = 1.0, 1.2, 1.4$. The contact value for the $\lambda = 1.2, 1.4$ cases is not shown. To be compared with Fig. 10 of Ref. [23]

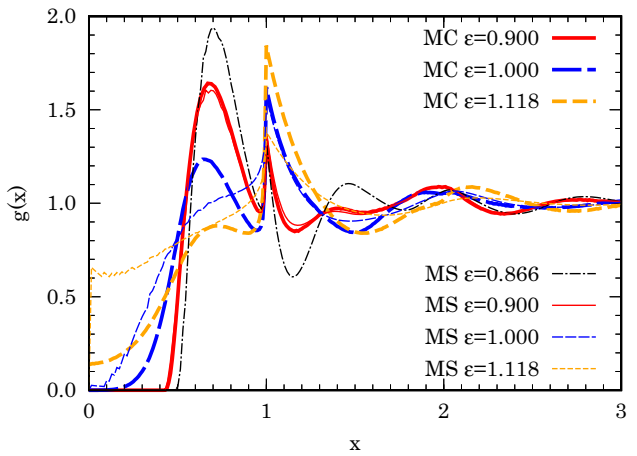

Fig. 11 LDF for $N = 100$ HD of radius $r_0 = 1$ with $\lambda = 1.2$ and $\epsilon = 0.9, 1.0, 1.118$. Comparison between our exact MC simulation (thick lines) and the theoretical approximate solution of Montero and Santos (MS) of Refs. [22,23] (thin lines). For the MS data, we also show the exact result at $\epsilon = \sqrt{3}/2$ already published in Fig. 5(a) of Ref. [23]. The remaining theoretical MS data were shared privately by A. Montero and was not published before

(a) $\epsilon = 4/5$, $r_0 = 6/5$ and (b) $\epsilon = \sqrt{7}/4$, $r_0 = 3/2$, with $|\beta\varphi_0| = 1$, and a surface density $\sigma = 6/10, 7/10$. Our results for the LDF, LSF, and RDF are shown in Figs. 12, 13, and 14, respectively. In Fig. 3, we show a snapshot of the simulation box for SW case (a) with $\sigma = 7/10$.

Our results show how the two cases SW and SS have very similar structures in the confined geometry under the nearest neighbor condition near close packing. The difference in structure between the two cases can be better seen at the level of the RDF where the SW produce a negative jump at $r = r_0$; whereas, the SS produce a positive jump as expected.

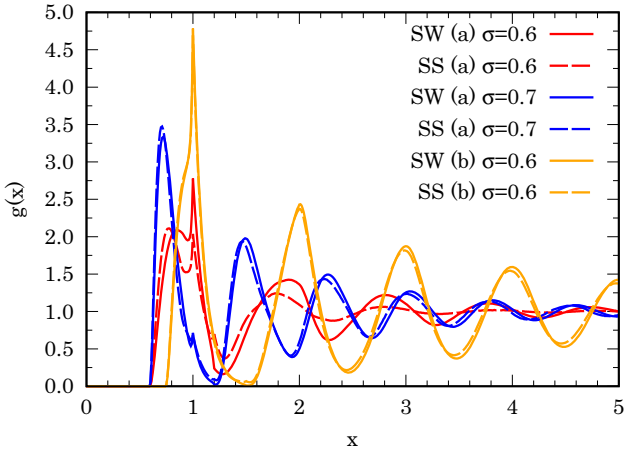

Fig. 12 LDF for $N = 100$ SW/SS cases **a** with $\sigma = 6/10, 7/10$ and **b** with $\sigma = 6/10$

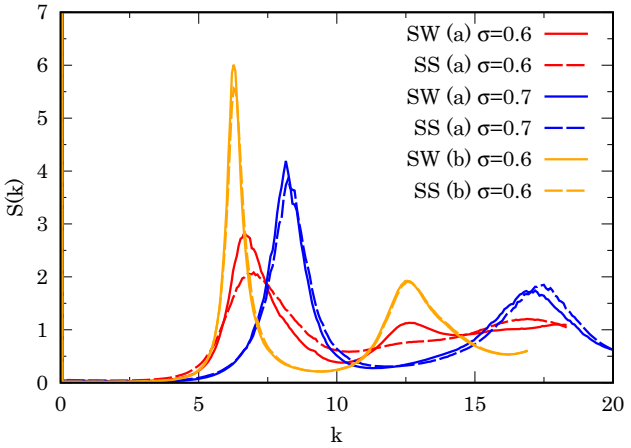

Fig. 13 LSF for $N = 100$ SW/SS cases **a** with $\sigma = 6/10, 7/10$ and **b** with $\sigma = 6/10$. We used $2n_{\max} + 1$ wave numbers with $n_{\max} = 270$

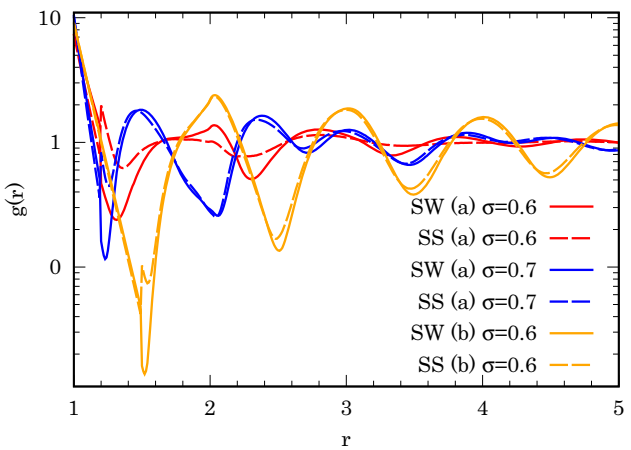

Fig. 14 RDF for $N = 100$ SW/SS cases **a** with $\sigma = 6/10, 7/10$ and **b** with $\sigma = 6/10$. Clearly $g(r) = 0$ for $r < 1$. Note the logarithmic scale on the ordinates

It would be an interesting project to explore how the *sticky limit* is approached in this constrained geometry [27–29, 42–46].

4 Conclusions

In this work, we performed Monte Carlo computer experiments to extract meta data for the thermodynamic and structural properties of hard-, square-well, and square-shoulder disks in narrow channels. We worked in the canonical ensemble. Our data are subject only to the statistical (we never used more than 10^9 single particle moves) and finite size errors (we used always 100 particles).

The novelty respect to previous studies relies in the use of the canonical ensemble instead of the isothermal isobaric one and in the study of both the radial and the linear distribution functions and of both the longitudinal and transverse pressures.

We compare our exact results for hard-disks with the semi-analytic ones of Montero and Santos [22,23] which are also exact in the nearest neighbor regime. We further compare our results with the results of the same authors but when the nearest neighbor condition is not met, making their solution just an approximation. In particular, we see how such theoretical solution ceases to be a good approximation as soon as the single file condition is violated.

Regarding the comparison with the works of Montero and Santos, it is important to point out that the "exact" approach of those authors is based on a mapping to a pure 1D system, while our simulations deal with a true (confined) 2D system. Thus, our results reinforce the exact character of their method.

We are aware that Montero and Santos are currently working at extending their theoretical framework to include the description of particles with a potential tail which would make possible the comparison with our Monte Carlo simulations of the square-Well and square-shoulder particles.

Acknowledgements. I am grateful to Ana M. Montero and Andrés Santos for proposing the project, stimulating its publication, and for the very many fruitful discussions and profound insights. I am grateful to Ana M. Montero for providing me with her results used in Figs. 1, 4, 8, 9, 11 some of which had not been published before.

Data availability This manuscript has no associated data or the data will not be deposited. [Authors' comment: The data that support the findings of this study are available from the corresponding author upon reasonable request.]

Declarations

Conflict of interest The author has no conflicts to disclose.

Appendix A: On the longitudinal pressure of HD from the LDF

Using the notation of Refs. [22,23], we have for the Equation Of State (EOS)

$$Z_{\rm L} = \frac{\beta p}{\lambda} = 1 + A^2 \sum_{i,j} \phi_i \phi_j a_{ij} e^{-\beta p a_{ij}}, \tag{A1}$$

where A^2 and ϕ_i are the solutions to

$$\sum_j e^{-\beta p a_{ij}} \phi_j = \frac{\beta p}{A^2} \phi_i. \tag{A2}$$

The LDF in the range $a(\epsilon) < x < 2a(\epsilon)$ is

$$g(x) = \frac{A^2}{\lambda} \sum_{i,j} \phi_i \phi_j a_{ij} e^{-\beta p x} \Theta(x - a_{ij}). \tag{A3}$$

Our aim is to express the EOS in terms of the integrals

$$I_n = \int_{a(\epsilon)}^1 {\rm d}x\, x^n g(x), \quad n = 0, 1 \tag{A4}$$

Inserting Eq. (A3) into Eq. (A4)

$$I_0 = \frac{A^2}{\beta p \lambda} \sum_{i,j} \phi_i \phi_j \left(e^{-\beta p a_{ij}} - e^{-\beta p} \right), \tag{A5a}$$

$$I_1 = \frac{A^2}{(\beta p)^2 \lambda} \sum_{i,j} \phi_i \phi_j \left[e^{-\beta p a_{ij}} (1 + \beta p a_{ij}) - e^{-\beta p} (1 + \beta p) \right]. \tag{A5b}$$

From Eq. (A2), we have $\sum_{i,j} \phi_i \phi_j e^{-\beta p a_{ij}} = \beta p / A^2$. Therefore,

$$\lambda I_0 = 1 - \frac{A^2}{\beta p} e^{-\beta p} \sum_{i,j} \phi_i \phi_j, \tag{A6a}$$

$$\beta p \lambda I_1 = 1 + A^2 \left[\sum_{i,j} \phi_i \phi_j a_{ij} e^{-\beta p a_{ij}} - e^{-\beta p} \left(1 + \frac{1}{\beta p} \right) \sum_{i,j} \phi_i \phi_j \right]. \tag{A6b}$$

Comparison with Eq. (A1) yields

$$\beta p \lambda I_1 = Z_{\rm L} - (1 + \beta p)(1 - \lambda I_0). \tag{A7}$$

This is a linear equation in $Z_{\rm L}$ which is solved by Eq. (2.13a) in the main text. From which immediately follows that for the pure 1D (Hard Rods) case, we find $Z_{\rm L} = 1/(1-\lambda)$, since $\epsilon \to 0$ and $a(\epsilon) \to 1$ so that $I_n = 0$, as it should be [16].

Note also that from Appendix C of Ref. [23] follows that in the $p \to \infty$ limit or equivalently in the $\lambda \to \lambda_{\rm cp}$ limit one finds $\lim_{\lambda \to \lambda_{\rm cp}} \lambda I_0 = \lim_{\lambda \to \lambda_{\rm cp}} \lambda^2 I_1 = 1$. In the continuum limit, one has from Eq. (A6a)

$$\lambda I_0 = 1 - \frac{e^{-\beta p}}{\ell} J^2, \tag{A8a}$$

$$J = \int_{-\epsilon/2}^{\epsilon/2} \phi(y)\, {\rm d}y. \tag{A8b}$$

In the high-pressure regime

$$\phi(y) \to \frac{1}{\sqrt{\mathcal{N}}}[\phi_+(y) + \phi_-(y)], \tag{A9a}$$

$$\phi_\pm(y) = e^{-a(y\pm\epsilon/2)\beta p}, \tag{A9b}$$

$$\mathcal{N} \to \frac{a(\epsilon)}{\epsilon\beta p} e^{-2a(\epsilon)\beta p}, \tag{A9c}$$

$$\ell \to \frac{a(\epsilon)}{2\epsilon\beta p} e^{-a(\epsilon)\beta p}. \tag{A9d}$$

Thus,

$$J = \frac{2}{\sqrt{\mathcal{N}}} \int_{-\epsilon/2}^{\epsilon/2} \phi_+(y)\, \mathrm{d}y. \tag{A10}$$

By expanding $a(y+\epsilon/2)$ around $y = \epsilon/2$

$$a(y+\epsilon/2) \to a(\epsilon) + \frac{\epsilon}{a(\epsilon)}(\epsilon/2 - y) + \cdots \tag{A11}$$

Therefore,

$$\begin{aligned} J &\to \frac{2}{\sqrt{\mathcal{N}}} e^{-a(\epsilon)\beta p} \int_{-\epsilon/2}^{\epsilon/2} e^{-\frac{\epsilon\beta p}{a(\epsilon)}(\epsilon/2-y)}\, \mathrm{d}y \\ &\to \frac{2}{\sqrt{\mathcal{N}}} e^{-a(\epsilon)\beta p} \frac{a(\epsilon)}{\epsilon\beta p} = 2\sqrt{\frac{a(\epsilon)}{\epsilon\beta p}}. \end{aligned} \tag{A12}$$

Consequently

$$\lambda I_0 \to 1 - 8e^{-\beta p[1-a(\epsilon)]}. \tag{A13}$$

Consistency between this result and Eq. (2.15) gives Eqs. (2.14a)–(2.14b) in the main text.

Appendix B: RDF of the ideal gas in a narrow channel

We arrive at the analytically exact Eq. (3.1) for the RDF of the ideal gas confined in the narrow channel with the following steps

$$\begin{aligned} g_{\mathrm{id}}(r) = \frac{\lambda}{2N} \int_0^L \mathrm{d}x_1 \int_0^L \mathrm{d}x_2 \int_{-\epsilon/2}^{\epsilon/2} \mathrm{d}y_1 \frac{1}{\epsilon} \int_{-\epsilon/2}^{\epsilon/2} \mathrm{d}y_2 \frac{1}{\epsilon} \\ \times \delta(r - \sqrt{(x_2-x_1)^2 + (y_2-y_1)^2}). \end{aligned} \tag{B1}$$

Since the integrand depends only on $x = |x_2 - x_1|$, we have $\int_0^L \mathrm{d}x_1 \int_0^L \mathrm{d}x_2 \ldots = 2\int_0^L \mathrm{d}x\,(L-x)\ldots$. Moreover,

$$\delta(r - \sqrt{x^2+s^2}) = \frac{r}{x}\delta(x - \sqrt{r^2-s^2}). \tag{B2}$$

Therefore,

$$\begin{aligned} &g_{\mathrm{id}}(r) \\ &= \frac{\lambda}{N\epsilon^2} r \int_{-\epsilon/2}^{\epsilon/2} \mathrm{d}y_1 \int_{-\epsilon/2}^{\epsilon/2} \mathrm{d}y_2 \left(\frac{L}{\sqrt{r^2-(y_2-y_1)^2}} - 1 \right) \\ &= \frac{2}{\epsilon^2} r \int_0^{\min(\epsilon,r)} ds\,(\epsilon - s) \left(\frac{1}{\sqrt{r^2-s^2}} - \frac{1}{L} \right) \\ &\approx \frac{2}{\epsilon^2} r \int_0^{\min(\epsilon,r)} ds\, \frac{\epsilon - s}{\sqrt{r^2-s^2}}. \end{aligned} \tag{B3}$$

Where in the first step, we have assumed that $\sqrt{r^2-(y_2-y_1)^2} < L$ and in the third step we have taken the limit $L \to \infty$. In the limit $r \gg 1$, $\sqrt{r^2-s^2} \approx r$, so that $g_{\mathrm{id}}(r) \approx 1$ as expected.

The integral in Eq. (B3) can be analytically performed and the result is given by Eq. (3.1) in the main text.

References

1. R. Fantoni, A. Santos, Multicomponent fluid of nonadditive hard spheres near a wall. Phys. Rev. E **87**, 042102 (2013). https://doi.org/10.1103/PhysRevE.87.042102
2. H. Kyakuno, K. Matsuda, H. Yahiro, Y. Inami, T. Fukuoka, Y. Miyata, K. Yanagi, Y. Maniwa, H. Kataura, T. Saito, M. Yumura, S. Iijima, Confined water inside single-walled carbon nanotubes: global phase diagram and effect of finite length. J. Chem. Phys. **134**, 244501 (2011)
3. M. Majumder, N. Chopra, B.J. Hinds, Mass transport through carbon nanotube membranes in three different regimes: ionic diffusion and gas and liquid flow. ACS Nano **5**, 3867 (2011)
4. D. Boda, W. Nonner, D. Henderson, B. Eisenberg, D. Gillespie, Volume exclusion in calcium selective channels. Biophys. J. **94**, 3486 (2008)
5. R. Fantoni, Exact results for one dimensional fluids through functional integration. J. Stat. Phys. **163**, 1247 (2016). https://doi.org/10.1007/s10955-016-1510-3
6. R. Fantoni, One-dimensional fluids with positive potentials. J. Stat. Phys. **166**, 1334 (2017). https://doi.org/10.1007/s10955-016-1707-5
7. R. Fantoni, How should we choose the boundary conditions in a simulation which could detect anyons in one and two dimensions? J. Low Temp. Phys. **202**, 247 (2021). https://doi.org/10.1007/s10909-020-02532-0
8. A. Santos, R. Fantoni, A. Giacometti, Penetrable square-well fluids: exact results in one dimension. Phys. Rev. E **77**, 051206 (2008). https://doi.org/10.1103/PhysRevE.77.051206
9. R. Fantoni, A. Giacometti, A. Malijevský, A. Santos, A numerical test of a high-penetrability approximation for the one-dimensional penetrable-square-well model. J. Chem. Phys. **133**, 024101 (2010). https://doi.org/10.1063/1.3455330
10. R. Fantoni, Non existence of a phase transition for the penetrable square well model in one dimension. J. Stat. Mech. (2010). https://doi.org/10.1088/1742-5468/2010/07/P07030
11. M.A.G. Maestre, R. Fantoni, A. Giacometti, A. Santos, Janus fluid with fixed patch orientations: theory and simulations. J. Chem. Phys. **138**, 094904 (2013). https://doi.org/10.1063/1.4793626
12. R. Fantoni, A. Giacometti, M.A.G. Maestre, A. Santos, Phase diagrams of janus fluids with up-down constrained orientations. J. Chem. Phys. **139**, 174902 (2013). https://doi.org/10.1063/1.4827861
13. R. Fantoni, M.A.G. Maestre, A. Santos, Finite-size effects and thermodynamic limit in one-dimensional janus fluids. J. Stat. Mech. (2021). https://doi.org/10.1088/1742-5468/ac2897
14. R. Fantoni, A. Santos, One-dimensional fluids with second nearest-neighbor interactions. J. Stat.

Phys. **169**, 1171 (2017). https://doi.org/10.1007/s10955-017-1908-6
15. A. Santos, *A Concise Course on the Theory of Classical Liquids. Basics and Selected Topics*, Lecture Notes in Physics, Vol. 923 (Springer, New York, 2016)
16. L. Tonks, The complete equation of state of one, two and three-dimensional gases of hard elastic spheres. Phys. Rev. **50**, 955 (1936)
17. Z.W. Salsburg, R.W. Zwanzig, J.G. Kirkwood, Molecular distribution functions in a one-dimensional fluid. J. Chem. Phys. **21** (1953)
18. R. Fantoni, B. Jancovici, G. Téllez, Pressures for a one-component plasma on a pseudosphere. J. Stat. Phys. **112**, 27 (2003). https://doi.org/10.1023/A:1023671419021
19. R. Fantoni, G. Téllez, Two dimensional one-component plasma on a flamm's paraboloid. J. Stat. Phys. **133**, 449 (2008). https://doi.org/10.1007/s10955-008-9616-x
20. R. Fantoni, Two component plasma in a flamm's paraboloid. J. Stat. Mech. (2012). https://doi.org/10.1088/1742-5468/2012/04/P04015
21. R. Fantoni, Jellium at finite temperature. Mol. Phys. **120**, 4 (2021). https://doi.org/10.1080/00268976.2021.1996648
22. A.M. Montero, A. Santos, Equation of state of hard-disk fluids under single-file confinement. J. Chem. Phys. **158**, 154501 (2023)
23. A.M. Montero, A. Santos, Structural properties of hard-disk fluids under single-file confinement. J. Chem. Phys. **159**, 034503 (2023)
24. A. Poncet, A. Grabsch, P. Illien, O. Bńichou, Generalized correlation profiles in single-file systems. Phys. Rev. Lett. **127**, 220601 (2021)
25. A. Horner, P. Pohl, Single-file transport of water through membrane channels. Faraday Discuss. **209**, 9 (2018)
26. R. Fantoni, A. Santos, Nonadditive hard-sphere fluid mixtures. A simple analytical theory. Phys. Rev. E **84**, 041201 (2011). https://doi.org/10.1103/PhysRevE.84.041201
27. R. Fantoni, D. Gazzillo, A. Giacometti, Stability boundaries, percolation threshold, and two phase coexistence for polydisperse fluids of adhesive colloidal particles. J. Chem. Phys. **122**, 034901 (2005). https://doi.org/10.1063/1.1831275
28. D. Gazzillo, R. Fantoni, A. Giacometti, Phase behavior of polydisperse sticky hard spheres: analytical solutions and perturbation theory. Mol. Phys. **104**, 3451 (2006). https://doi.org/10.1080/00268970601050892
29. R. Fantoni, D. Gazzillo, A. Giacometti, P. Sollich, Phase behavior of weakly polydisperse sticky hard spheres: perturbation theory for the percus-yevick solution. J. Chem. Phys. **125**, 164504 (2006). https://doi.org/10.1063/1.2358136
30. D.A. Kofke, A.J. Post, Hard particles in narrow pores. Transfer-matrix solution and the periodic narrow box. J. Chem. Phys. **98**, 4853 (1993)
31. K.K. Mon, Analytical evaluation of third and fourth virial coefficients for hard disk fluids in narrow channels and equation of state. Phys. A **556**, 124833 (2020)
32. S. Varga, G. Balló, P. Gurin, Structural properties of hard disks in a narrow tube. J. Stat. Mech. (2011)
33. A. Huerta, T. Bryk, V.M. Pergamenshchik, A. Trokhymchuk, Collective dynamics in quasi-one-dimensional hard disk system. Front. Phys. **9**, 636052 (2021)
34. M.H. Kalos, P.A. Whitlock, *Monte Carlo Methods* (Wiley, New York, 1986)
35. M.P. Allen, D.J. Tildesley, *Computer Simulation of Liquids* (Oxford University Press, Oxford, 1987). (**Section 6.2**)
36. D. Frenkel, B. Smit, *Understanding Molecular Simulation* (Academic Press, San Diego, 1996)
37. J.-P. Hansen, I.R. McDonald, *Theory of Simple Liquids*, 2nd edn. (Academic Press, San Diego, 1986). (**Section 2.5**)
38. A.M. Montero, private communication (2023)
39. V.M. Pergamenshchik, Analytical canonical partition function of a quasi-one-dimensional system of hard disks. J. Chem. Phys. **153**, 144111 (2020)
40. A. Santos, private communication (2023)
41. Y. Hu, P. Charbonneau, Kosterlitz-thouless-type caging-uncaging transition in a quasi-one-dimensional hard disk system. Phys. Rev. Res. **3**, 038001 (2021)
42. R. Fantoni, D. Gazzillo, A. Giacometti, The thermodynamic instabilities of a binary mixture of sticky hard spheres. Phys. Rev. E **72**, 011503 (2005). https://doi.org/10.1103/PhysRevE.72.011503
43. D. Gazzillo, A. Giacometti, R. Fantoni, P. Sollich, Multicomponent adhesive hard sphere models and short-ranged attractive interactions in colloidal or micellar solutions. Phys. Rev. E **74**, 051407 (2006). https://doi.org/10.1103/PhysRevE.74.051407
44. R. Fantoni, D. Gazzillo, A. Giacometti, M.A. Miller, G. Pastore, Patchy sticky hard spheres: analytical study and Monte Carlo simulations. J. Chem. Phys. **127**, 234507 (2007). https://doi.org/10.1063/1.2805066
45. R. Fantoni, Andersen-weeks-chandler perturbation theory and one-component sticky-hard-spheres. J. Stat. Phys. **168**, 652 (2017). https://doi.org/10.1007/s10955-017-1810-2
46. R. Fantoni, Effect of quantum dispersion on the radial distribution function of a one-component sticky-hard-sphere fluid. J. Stat. Mech. (2018). https://doi.org/10.1088/1742-5468/aab690